Available online at www.sciencedirect.com
SCIENCE DIRECT®
Journal of Solid State Chemistry 175 (2003) 188–196
JOURNAL OF SOLID STATE CHEMISTRY
http://elsevier.com/locate/jssc

Synthesis and characterization of the reduced double-layer manganite $Sr_3Mn_2O_{6+x}$

L.J. Gillie,[a] A.J. Wright,[a] J. Hadermann,[b] G. Van Tendeloo,[b] and C. Greaves[a,*]

[a] *School of Chemical Sciences, University of Birmingham, Edgbaston, Birmingham B15 2TT, UK*
[b] *EMAT, RUCA, Groenenborgerlaan 171, Antwerp 2020, Belgium*

Received 25 February 2003; received in revised form 17 April 2003; accepted 25 April 2003

Abstract

The oxygen-deficient Ruddlesden–Popper (RP) phase $Sr_3Mn_2O_6$ crystallizes with an ordered array of oxygen vacancies to afford a structure in which the Mn^{3+} ions exist in a square-pyramidal environment. The MnO_5 polyhedra are linked through their corners to form a structure that is related to that observed for the single-layered material, $Sr_2MnO_{3.5}$. The nuclear and magnetic structures of a polycrystalline sample of $Sr_3Mn_2O_6$ have been determined using Rietveld analysis of neutron powder diffraction data and electron diffraction techniques. The pure Mn^{3+} double-layered phase crystallizes in a superstructure of the simple RP subcell: tetragonal, $P4/mbm$, $a = 10.8686(2)$ Å and $c = 20.2051(3)$ Å.

Magnetic susceptibility studies suggest a transition at ~ 250 K to a canted antiferromagnetic ordered structure. The magnetic unit-cell consists of ferromagnetic clusters of corner-sharing MnO_5 units, which are antiferromagnetically aligned to other clusters within the layers.

1. Introduction

The magnetotransport properties of low-dimensional solids containing manganese in a mixed Mn^{3+}/Mn^{4+} oxidation state have been the subject of much research since the discovery of low-field negative magnetoresistance in $La_{1.2}Sr_{1.8}Mn_2O_7$ [1]. In this phase, which is a member of the $n = 2$ double-layered Ruddlesden–Popper (RP) series, the Mn^{3+}/Mn^{4+} cations allow double-exchange within the perovskite block layers to give ferromagnetic order below 126 K [1,2].

The parent oxide $Sr_3Mn_2O_7$ has been studied extensively and exhibits a large degree of oxygen non-stoichiometry [3–7]. Mitchell et al. [4] have reported an oxygen-deficient phase, $Sr_3Mn_2O_{6.55}$, in which the vacancies do not form an ordered superstructure, but are located exclusively within the equatorial positions in the "MnO_2" layers. However, the pure Mn^{3+} single-layered analog, $Sr_2MnO_{3.5}$ has been reported to have an ordered array of vacancies [8]. The phase $Sr_3Mn_2O_6$ is the focus of this study, since its oxygen content corresponds to the removal of one oxygen anion per Mn-polyhedron, precisely the situation found in $Sr_2MnO_{3.5}$ so that one might expect its structure to contain an ordered array of square pyramidally coordinated Mn cations.

The oxygenated material, $Sr_3Mn_2O_7$ orders antiferromagnetically below a Néel temperature of $T_N = 160$ K. The Mn magnetic moments are aligned along +[001] and –[001], and the magnetic unit-cell requires a doubling along the [100] direction of the nuclear unit-cell, since each spin is oriented antiparallel to its five neighboring spins. The oxygen-deficient phase $Sr_3Mn_2O_{6.55}$ does not order magnetically above 20 K although a mixed Mn^{3+}/Mn^{4+} oxidation state is present. There is no evidence for the double-exchange ferromagnetism that is often observed for colossal magnetoresistive manganites, and this has been attributed to oxygen vacancy disorder causing frustration in all possible long-range magnetic exchange pathways [4]. It was recognized, however, that if an ordered arrangement could be achieved, then this magnetic frustration might be relieved [4]. $Sr_3Mn_2O_{6.55}$ is also reported to be highly resistive and this could arise from the mixed octahedral and square-pyramidal environments trapping any itinerant e_g electrons. In this study, we report that removal of additional oxygen from $Sr_3Mn_2O_{6.55}$

*Corresponding author. Fax: +44-121-414-4442.
E-mail address: c.greaves@bham.ac.uk (C. Greaves).

0022-4596/03/$ - see front matter © 2003 Elsevier Inc. All rights reserved.
doi:10.1016/S0022-4596(03)00245-7

allows formation of an ordered vacancy arrangement within the perovskite block layers, in which the corner linked MnO_5 polyhedra form similar elongated pseudo-hexagonal channels, to those in $Sr_2MnO_{3.5}$ (Fig. 1).

2. Experimental

The oxygen-deficient phase $Sr_3Mn_2O_6$ was prepared via ceramic synthesis using stoichiometric proportions of high-purity $SrCO_3$ and Mn_2O_3. The powder mixture was pressed into a pellet and heated in N_2 gas at 1350°C for 48 h, with an intermediate grinding to yield a single-phase sample. The oxygen content of this "as-synthesized" phase was approximately $Sr_3Mn_2O_{6.3}$ but oxygen stoichiometries down to $Sr_3Mn_2O_{6.15(1)}$ could be attained upon further calcination in flowing N_2 gas. The samples could then be reduced to the pure Mn^{3+} phase, $Sr_3Mn_2O_6$ upon low-temperature annealing in a gaseous mixture of H_2/N_2 gas ($10\%H_2/90\%N_2$) at 590°C for 10 h. Reductive decomposition of $Sr_3Mn_2O_{6+x}$ at 1000°C in a mixture of $10\%H_2/90\%N_2$ gas (to form SrO and MnO), and oxidation in a stream of O_2 at 400°C (to form $Sr_3Mn_2O_7$) provided confirmation of the oxygen contents of both "as-synthesized" and reduced samples. The nature of the decomposition products was confirmed by X-ray powder diffraction (XRPD).

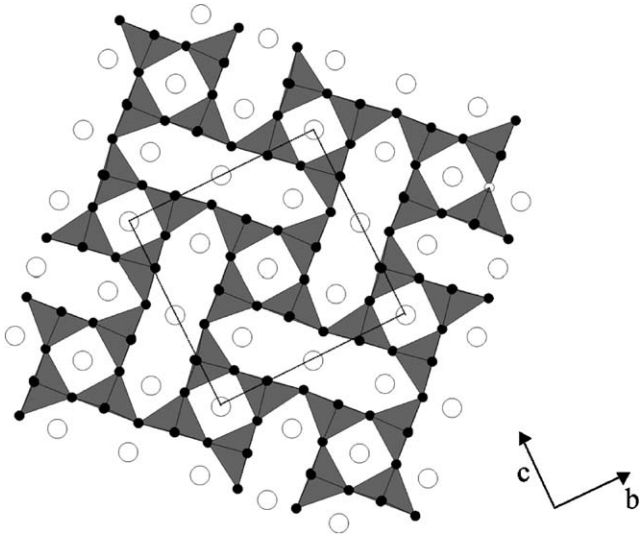

Fig. 1. Crystallographic structure of a perovskite block layer of $Sr_2MnO_{3.5}$ (monoclinic, $a = 6.85$ Å, $b = 10.81$ Å, $c = 10.81$ Å, $\beta = 113.2°$ [8]). Gray polyhedra are MnO_5 units; black spheres are oxygen polyhedral ligands and white spheres are Sr^{2+} cations.

XRPD data were collected with a Siemens D5000 diffractometer (monochromated Cu$K\alpha_1$ radiation source, position sensitive detector, transmission mode). Neutron powder diffraction (NPD) profiles were recorded on the high-resolution powder diffractometer D2B at Institut Laue-Langevin, Grenoble (wavelength 1.594 Å, Ge monochromator). Rietveld structural refinements were carried out with the GSAS package [9]. Electron diffraction and high-resolution electron microscopy were performed with a Philips CM20 microscope and a JEOL 4000 EX Electron Microscope. The magnetic susceptibility of the sample was measured with a Quantum Design Physical Property Measurement System. Both zero-field cooled (ZFC) and field-cooled (FC) measurements were carried out under an applied

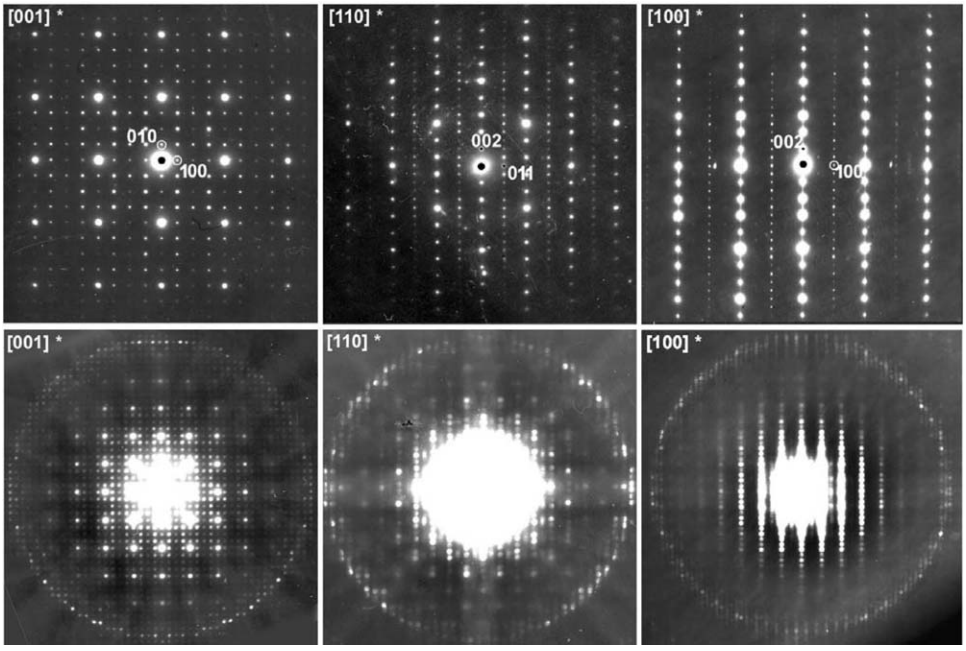

Fig. 2. SAED (top row) and microdiffraction patterns (bottom row) from the main zones of $Sr_3Mn_2O_6$, with indices referring to the supercell, $a = b = 2\sqrt{2}a_0, c = c_0$. For better visualization of the FOLZ the microdiffraction patterns are at different scales.

field of 1000 G. Thermogravimetric (TG) measurements were recorded on a Rheometric Scientific STA 1500 Simultaneous Thermal Analyzer.

3. Results and discussion

Preliminary structural studies were based on XRPD data, which were collected over a period of several hours. In accordance with previous reports, a body-centered tetragonal model was adopted for the refinement using the space-group $I4/mmm$ with lattice parameters $a = 3.8565(1)$ Å and $c = 20.2796(7)$ Å. This confirmed the presence of the oxygen vacancies exclusively in the equatorial positions of the perovskite block layers, in agreement with the structure reported by Mitchell et al. [4,6]. There was no evidence of superstructure, but XRPD is not particularly reliable for the precise determination of oxygen structural parameters, and it was assumed that subtle structural changes may remain undetected. Although the structure refinement was reasonable, more sensitive probes for oxygen order were employed to assess the reliability of this basic disordered model.

In contrast to the XRPD study, the electron diffraction (ED) experiments showed clear evidence of a superstructure. The SAED patterns (Fig. 2, top row) could be indexed on a tetragonal cell with a basal plane of ca. 10.8×10.8 Å, $(2\sqrt{2}a_0 \times 2\sqrt{2}a_0$, where a_0 is the simple sub-cell parameter), and c parameter $c = c_0 = 20.3$ Å. The net symmetry of the supercell could be determined from the microdiffraction patterns (Fig. 2, bottom row) as P-b-, which leaves three possible spacegroups $P4bm$, $P\bar{4}b2$ and $P4/mbm$. On the high-resolution electron microscopy (HREM) images, shown in Fig. 3, the superstructure is almost invisible to the eye; the images are at first sight equivalent to those one would have for the basic cell, showing that the stacking of the cation layers is the same in the supercell as in the basic one. However, upon taking Fourier transforms of the images (shown as insets in Fig. 3) it is clear that the same superstructure as was observed for the ED patterns is indeed present in the HREM images.

The ED patterns strongly suggest a similar type of vacancy order to that observed in the $n = 1$ material, $Sr_2MnO_{3.5}$ [8], and hence a similar ordering pattern within the $MnO_{1.5}$ layers was proposed (Fig. 1). There was no evidence for any change in the c-parameter, so a tetragonal space group was sought in which a $10 \times 10 \times 20$ Å cell would permit a superstructure with elongated hexagonal channels. It was assumed that within each double perovskite block, the vacancies would be located in identical positions for each

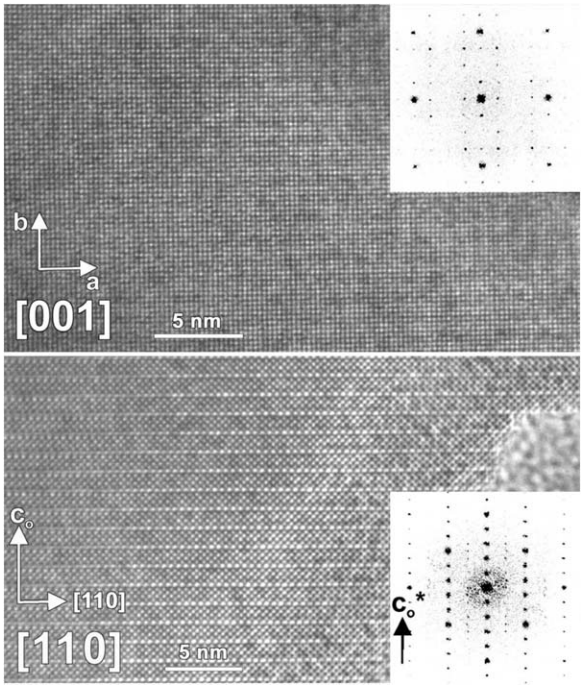

Fig. 3. [001] (top) and [110] (bottom) HREM images of $Sr_3Mn_2O_6$, with their Fourier transforms. Indicated axes are according to the supercell, $a = b = 2\sqrt{2}a_0, c = c_0$.

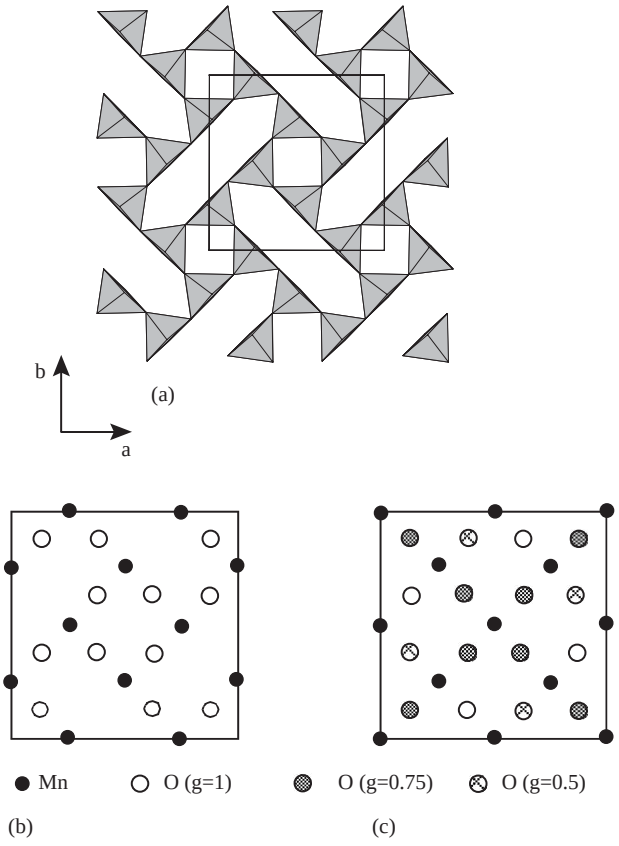

Fig. 4. (a) Proposed linking of MnO_5 square pyramids in the $MnO_{1.5}$ layers near $z = 0$; the unit cell is outlined. (b) The positions of the Mn and O atoms in the $MnO_{1.5}$ layers near $z = 0$. (c) The result of translating the layers shown in (b) by $\pm\frac{1}{4}[100]$ and $\pm\frac{1}{4}[010]$ to generate layers at $z \sim \frac{1}{2}$. The O atom site occupancies (g) are indicated.

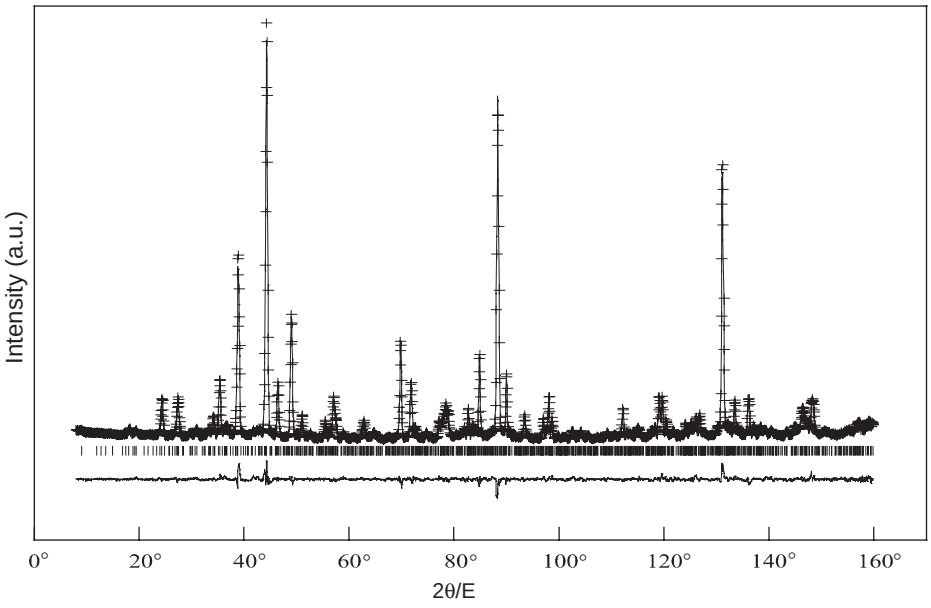

Fig. 5. Observed (+), calculated and difference NPD profiles of $Sr_3Mn_2O_{6+x}$ at 300 K. Tick marks show diffraction peak positions for nuclear structure.

Table 1
Rietveld refinement results for $Sr_3Mn_2O_{6+x}$ from NPD data at 300 K

Atom	Position	x	y	z	$U_{iso} \times 100/Å^2$	g
Mn1	16*l*	0.4999(7)	0.7526(6)	0.0960(1)	0.31(4)	1
Mn2	4*f*	0.5	0	0.5960(1)	0.31(4)	1
Mn3	8*k*	0.2467(1)	0.2533(9)	0.5960(1)	0.31(4)	1
Mn4	4*e*	0.5	0.5	0.5960(1)	0.31(4)	1
Sr1	8*j*	0.5132(7)	0.7514(9)	0.5	0.96(3)	1
Sr2	2*d*	0.5	0	0	0.96(3)	1
Sr3	16*l*	0.5054(7)	0.7499(7)	0.3139(3)	0.96(3)	1
Sr4	4*f*	0.5	0	0.8118(8)	0.96(3)	1
Sr5	4*g*	0.2462(2)	0.2538(3)	0	0.96(3)	1
Sr6	2*a*	0.5	0.5	0	0.96(3)	1
Sr7	8*k*	0.2421(7)	0.2579(7)	0.8171(6)	0.96(3)	1
Sr8	4*e*	0.5	0.5	0.8191(8)	0.96(3)	1
O1	8*i*	0.5210(1)	0.7700(1)	0	1.21(3)	1
O2	2*c*	0.5	0	0.5	1.21(3)	1
O3	16*e*	0.5123(8)	0.7554(7)	0.1921(4)	1.21(3)	1
O4	4*f*	0.5	0	0.6910(1)	1.21(3)	1
O5	8*k*	0.641(4)	0.859(4)	0.0945(1)	1.21(3)	0.20 (3)
O6	8*k*	0.3660(1)	0.8660(1)	0.5936(1)	1.21(3)	0.58(1)
O7	8*k*	0.3926(7)	0.8926(7)	0.0945(1)	1.21(3)	1
O8	8*k*	0.6218(9)	0.8782(9)	0.5945(1)	1.21(3)	1
O9	4*h*	0.2330(1)	0.2673(2)	0.5	1.21(3)	1
O10	2*b*	0.5	0.5	0.5	1.21(3)	1
O11	8*k*	0.2495(8)	0.2505(8)	0.6910(1)	1.21(3)	1
O12	4*e*	0.5	0.5	0.6901(1)	1.21(3)	1
O13	16*l*	0.8637(7)	0.1420(7)	0.0945(1)	1.21(3)	1
O14	16*l*	0.1190(1)	0.1293(9)	0.5945(1)	1.21(3)	0.72(2)

Space group $P4/mbm$; $a = 10.8686(2)$ Å; $c = 20.2051(3)$ Å; $\chi^2 = 3.930$; $R_{wp} = 4.95\%$ and $R_p = 3.93\%$.

Mn-containing sheet, in accordance with the order observed in the vacancy ordered perovskite, $SrMnO_{2.5}$ [10,11]. However, no fully ordered model—in which the bilayer of square pyramids at $z = \frac{1}{2}$ can be obtained from a simple translation of the layers at $z = 0$ and 1—is compatible with tetragonal symmetry. Using $Sr_2MnO_{3.5}$

Table 2
Selected Mn–O bond lengths from 300 K NPD data for $Sr_3Mn_2O_{6+x}$

Mn–O bond lengths (Å)			
Mn1–O1	1.963(3)	Mn2–O8 (× 2)	1.87(1)
Mn1–O3	1.945(9)	Mn3–O6	1.73(2)[a]
Mn1–O5	1.92(1)[a]	Mn3–O8	2.02(2)
Mn1–O7	1.916(8)	Mn3–O9	1.952(4)
Mn1–O13	1.91(1)	Mn3–O11	1.91(2)
Mn1–O13	1.99(1)	Mn3–O14 (× 2)	1.94(1)[a]
Mn2–O2	1.940(3)	Mn4–O10	1.940(3)
Mn2–O4	1.91(2)	Mn4–O12	1.90(2)
Mn2–O6 (× 2)	2.07(2)[a]	Mn4–O14 (× 2)	1.91(1)

[a] Represents Mn–O bond lengths where the oxygen site is only partially occupied.

Table 3
Selected O–Mn–O bond angles from 300 K NPD data of $Sr_3Mn_2O_{6+x}$

O–Mn–O bond angles (deg)[a]			
O1–Mn1–O3	167.5(6)	O7–Mn1–O13	166.3(5)
O1–Mn1–O7	88.9(4)	O7–Mn1–O13	92.0(6)
O1–Mn1–O13	87.2(5)	O13–Mn1–O13	101.6(5)
O1–Mn1–O13	97.7(4)	O2–Mn2–O8 (× 2)	89.0(1)
O3–Mn1–O7	92.7(4)	O4–Mn2–O8 (× 2)	91.0(1)
O3–Mn1–O13	88.4(4)	O8–Mn3–O9	95.4(7)
O3–Mn1–O13	94.6(3)	O8–Mn3–O11	175.0(1)

[a] Only bond angles where the oxygen site is fully occupied are given.

as a model, the probable translation would correspond to $\frac{1}{4}$[100] (or the equivalent $\frac{1}{4}$[010]), but this would result in monoclinic symmetry, as observed in $Sr_2MnO_{3.5}$. In addition, for orthogonal axes, the repeat period along [001] would produce a supercell with doubled c. No evidence for this was apparent from the ED patterns, nor from the HREM images. It is interesting to note, however, that a structure in which the bilayer at $z = \frac{1}{2}$ consists of a statistical mixture of the four equivalent translations, $\pm\frac{1}{4}$[100] and $\pm\frac{1}{4}$[010], would have the required tetragonal symmetry, and such a model was therefore used as a basis for NPD structural analysis; the possible nature of the disorder will be considered later.

NPD profiles were recorded at both ambient temperature and 2 K. Fig. 4 illustrates the starting model for refinement. Fig. 4a shows the linking of the square pyramids in the bilayer at $z = 0$, in accordance with the order previously reported for $Sr_2MnO_{3.5}$ Fig. 1, and Fig. 4b shows a simplified view of the Mn and O positions in these layers. Fig. 4c shows the effect of translating the atoms in a statistical fashion along the four equivalent directions $\pm\frac{1}{4}$[100] and $\pm\frac{1}{4}$[010]: in this way, the layers at $z \sim \frac{1}{2}$ are generated and contain O sites with occupancies of $g = 1$, 0.75 and 0.5. A space-group that is consistent with such vacancy-ordering is $P4/mbm$ with lattice parameters $a \sim 10.86$ Å and $c \sim 20.21$ Å. A Rietveld structure refinement (Fig. 5), was performed on

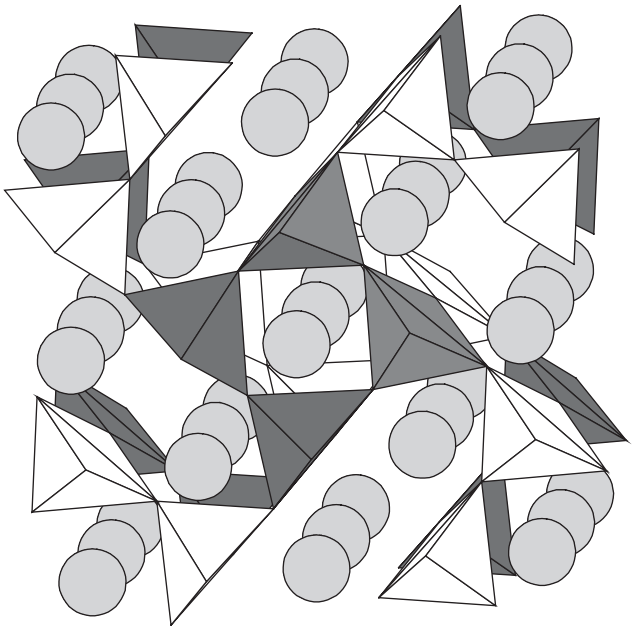

Fig. 6. Magnetic structure of $Sr_3Mn_2O_6$ in the $z = 0$ and 1 layers. White polyhedra have a net moment "spin up" and gray polyhedra have a net moment "spin down". (White and gray polyhedra are MnO_5 units and light gray spheres are Sr^{2+} cations. Oxygen polyhedral ligands have been omitted for clarity.)

the data collected at 300 K in order to confirm the nuclear structure before considering the nature of any magnetic order. In order to simplify the refinement, only three isotropic thermal factors were used: one each for Mn, Sr and O. Using a 36-point linear interpolated background with a pseudo-Voigt peak shape function, the refinement proceeded smoothly and converged with $\chi^2 = 3.930$, and reliability factors $R_{wp} = 4.95\%$ and $R_p = 3.93\%$ (see Tables 1–3); the NPD profiles are shown in Fig. 5. For purposes of comparison, refinement was also performed using the disordered $I4/mmm$ subcell model, but this produced significantly worse agreement between the observed and calculated patterns ($\chi^2 = 10.49$; $R_{wp} = 8.12\%$; $R_p = 6.09\%$).

For an ideal stoichiometry of $Sr_3Mn_2O_6$, O5 would have $g = 0$, and O6/O14 in the layers either side of $z = \frac{1}{2}$ would have $g = 0.5$ and 0.75, respectively. The data are therefore in good agreement with the proposed model, but suggest the possibility of a small degree of aerial oxidation, since the refinement corresponds to a composition of $Sr_3Mn_2O_{6.11(3)}$; similar oxidation was found to occur in $Sr_2MnO_{3.5}$. The bond distances and angles given in Tables 2 and 3 have limited significance for Mn2, Mn3 and Mn4, since these ions are within the layers at $z = \frac{1}{2}$, and stereochemical information is restricted by the disordered nature of these layers. However, Mn1 is located in the fully ordered layers, and the longest bond, Mn1–O13 [1.99(1) Å] corresponds to the apical bond of the square pyramids. The other Mn1–O13 bond [1.91(1) Å], and Mn1–O7 [1.916(8) Å],

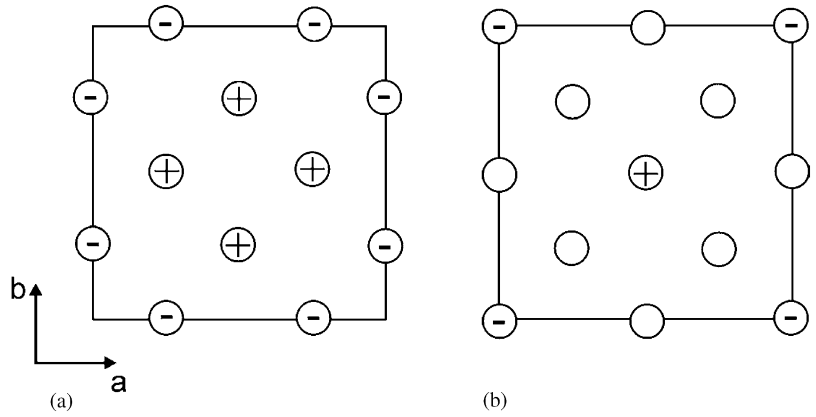

Fig. 7. (a) The Mn ions with superposed magnetic spin directions in the layer with $z = 0.09$. (b) Translation of the layer shown in (a) by $\pm\frac{1}{4}[100]$ and $\pm\frac{1}{4}[010]$ results in cancellation of 3/4 of the moments, leaving $\frac{1}{8}$ with spin up and $\frac{1}{8}$ with spin down.

Table 4
Rietveld refinement results for $Sr_3Mn_2O_6$ from NPD data at 2 K

Atom	Position	x	y	z	$U_{iso} \times 100/Å^2$	g
Mn1	16*l*	0.5010(1)	0.7531(5)	0.0954(4)	0[a]	1
Mn2	4*f*	0.5	0	0.5872(9)	0[a]	1
Mn3	8*k*	0.2477(1)	0.2525(1)	0.5949(9)	0[a]	1
Mn4	4*e*	0.5	0.5	0.6036(8)	0[a]	1
Sr1	8*j*	0.5106(8)	0.7460(7)	0.5	0.56(3)	1
Sr2	2*d*	0.5	0	0	0.56(3)	1
Sr3	16*l*	0.5086(6)	0.7524(5)	0.3157(2)	0.56(3)	1
Sr4	4*f*	0.5	0	0.8127(8)	0.56(3)	1
Sr5	4*g*	0.2450(1)	0.2556(1)	0	0.56(3)	1
Sr6	2*a*	0.5	0.5	0	0.56(3)	1
Sr7	8*k*	0.2430(7)	0.2570(7)	0.8143(7)	0.56(3)	1
Sr8	4*e*	0.5	0.5	0.8182(8)	0.56(3)	1
O1	8*i*	0.5267(9)	0.7727(8)	0	0.91(2)	1
O2	2*c*	0.5	0	0.5	0.91(2)	1
O3	16*e*	0.5089(8)	0.7545(5)	0.1933(3)	0.91(2)	1
O4	4*f*	0.5	0	0.6915(9)	0.91(2)	1
O5	8*k*	0.611(3)	0.889(3)	0.095(3)	0.91(2)	0.19(1)
O6	8*k*	0.366(1)	0.896(1)	0.593(1)	0.91(2)	0.60(1)
O7	8*k*	0.3934(6)	0.8934(6)	0.0956(6)	0.91(2)	1
O8	8*k*	0.622(1)	0.878(1)	0.5976(6)	0.91(2)	1
O9	4*h*	0.244(1)	0.256(1)	0.5	0.91(2)	1
O10	2*b*	0.5	0.5	0.5	0.91(2)	1
O11	8*k*	0.2407(8)	0.2593(8)	0.6885(7)	0.91(2)	1
O12	4*e*	0.5	0.5	0.6887(9)	0.91(2)	1
O13	16*l*	0.8654(7)	0.1387(7)	0.0931(4)	0.91(2)	1
O14	16*l*	0.1179(9)	0.1354(9)	0.5943(5)	0.91(2)	0.80(1)

[a] Denotes where thermal factors were fixed; thermal factors were constrained to give sensible results; Space group $P4/mbm$; $a = 10.8354(2)$ Å; $c = 20.1683(3)$ Å; $\chi^2 = 8.5103$; $R_{wp} = 5.00\%$ and $R_p = 3.92\%$.

are the equatorial bonds in the Mn planes, whilst the bonds to O1 and O3 correspond to the equatorial bonds directed approximately along [001].

NPD data collected at 2 K clearly revealed additional low intensity peaks at low angle, which were attributed to the presence of antiferromagnetic (AFM) ordering. As in the case of $Sr_2MnO_{3.5}$ [8], the magnetic structure was predicted in accordance with the Goodenough–Kanamori rules for superexchange interactions [12,13]. For the $z = 0$ and 1 layers, the magnetic interactions could be predicted by considering the interactions between two empty dx^2-y^2 orbitals (to give AFM exchange) and between a half-filled dz^2 orbital and an empty dx^2-y^2 orbital (giving ferromagnetic (FM) exchange). This leads to the formation of four ferromagnetically aligned MnO_5 units, which are surrounded, within each single perovskite layer, by four other similar clusters that are antiferromagnetically

aligned to it. The double perovskite block layers are comprised of blocks of ferromagnetic clusters stacking directly on top of each other that have net opposite spins (Fig. 6). For the layers near $z = \frac{1}{2}$, the statistical superposition of $z = 0$ layers translated by $\pm\frac{1}{4}[100]$ and $\pm\frac{1}{4}[010]$ results in a situation in which $\frac{1}{8}$ of the ions will have spin up, $\frac{1}{8}$ spin down and the spins of $\frac{3}{4}$ of the Mn ions will cancel, as shown in Fig. 7.

Table 5
Selected Mn–O bond lengths from 2 K NPD data for $Sr_3Mn_2O_6$

Mn–O bond lengths (Å)			
Mn1–O1	1.96(9)	Mn2–O8 (× 2)	1.89(2)
Mn1–O3	1.97(9)	Mn3–O6	1.74(2)[a]
Mn1–O5	1.90(1)[a]	Mn3–O8	1.99(2)
Mn1–O7	1.92(8)	Mn3–O9	1.91(2)
Mn1–O13	1.91(1)	Mn3–O11	1.89(2)
Mn1–O13	1.98(1)	Mn3–O14 (× 2)	1.89(1)[a]
Mn2–O2	1.76(2)	Mn4–O10	2.09(2)
Mn2–O4	2.10(3)	Mn4–O12	1.71(2)
Mn2–O6 (× 2)	2.06(2)[a]	Mn4–O14 (× 4)	1.95(1)[a]

[a] Represents Mn–O bond lengths where the oxygen site is only partially occupied.

Table 6
Selected O–Mn–O bond angles from 2 K NPD data of $Sr_3Mn_2O_6$

O–Mn–O bond angles (deg)[a]			
O1–Mn1–O3	167.3(6)	O7–Mn1–O13	92.9(6)
O1–Mn1–O7	90.1(6)	O13–Mn1–O13	99.1(5)
O1–Mn1–O13	86.4(6)	O2–Mn2–O8 (× 2)	96.3(7)
O1–Mn1–O13	99.0(5)	O4–Mn2–O8 (× 2)	83.7(7)
O3–Mn1–O7	91.1(6)	O8–Mn2–O8	167.3(1)
O3–Mn1–O13	89.8(5)	O8–Mn3–O9	93.2(9)
O3–Mn1–O13	93.6(5)	O8–Mn3–O11	91.6(9)
O7–Mn1–O13	167.9(6)	O9–Mn3–O11	175.2(1)

[a] Only bond angles where the oxygen site is fully occupied are given.

A Rietveld refinement of the 2 K data was therefore performed using the nuclear model established from the 300 K data and the magnetic order described above. Constraints to thermal factors were similar to those used for the 300 K data, but since U_{iso} for Mn refined to a slightly negative value, it was constrained to zero. The refinement confirmed that the magnetic scattering was consistent with the predicted magnetic structure, and indicated that the manganese spins were oriented at an angle to the c-axis, with the components of the manganese moments being $M_x = 2.04(3)\,\mu_B$ and $M_z = 2.36(4)\,\mu_B$. The resultant moment of $3.12(4)\,\mu_B$ compares with the ideal value of $4\,\mu_B$ for Mn^{3+} ions, in the absence of covalent and quantum effects. Refinement results and selected bond lengths and angles are given in Tables 4–6, and the final fitted NPD profiles are shown in Fig. 8. The magnetic unit-cell showing the orientation of the Mn moments is given in Fig. 9. As for $Sr_2MnO_{3.5}$ [8], the refinement suggested that the moments for the Mn ions in the layers around $z = \frac{1}{2}$ are not collinear with those for the ions near $z = 0$. However, it must be stressed that the magnetic reflections are very weak, and the relative orientation of the moments between the bilayers should be regarded as tentative. Nevertheless, it is clear that the nuclear structure, and the basic magnetic order which can be

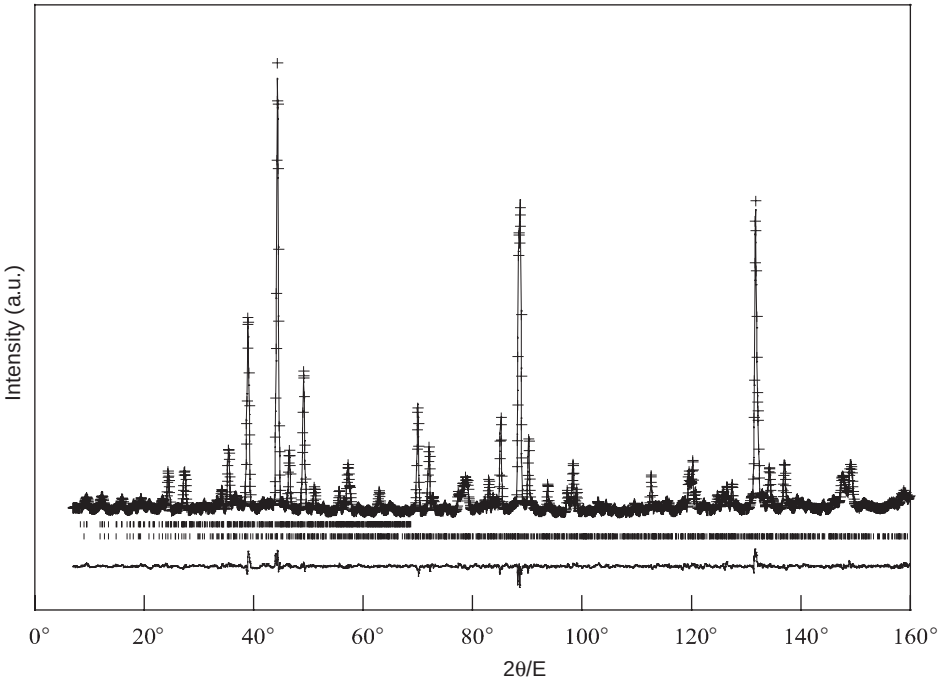

Fig. 8. Observed (+), calculated and difference NPD profiles of $Sr_3Mn_2O_{6+x}$ at 2 K. Upper tick marks represent diffraction peak positions for magnetic structure and lower tick marks are those of nuclear structure.

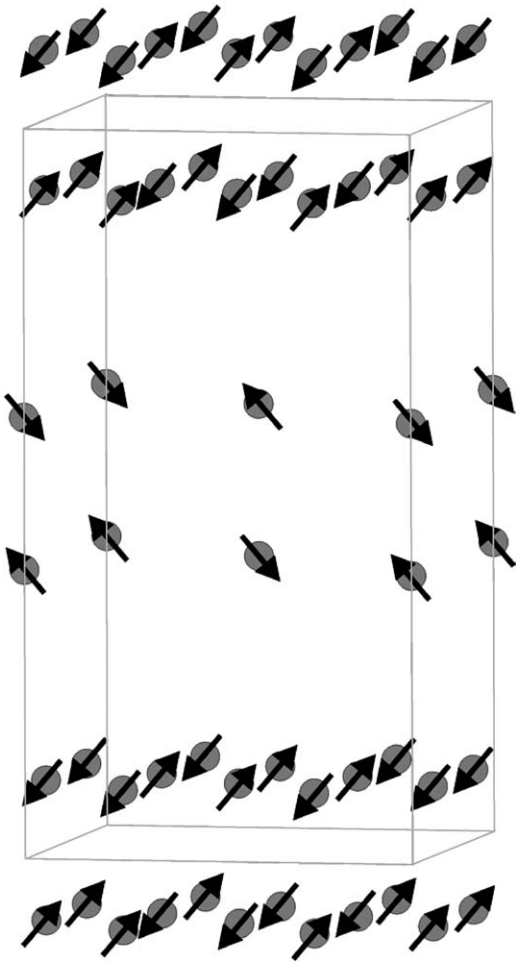

Fig. 9. Magnetic structure of $Sr_3Mn_2O_6$ determined from 2 K NPD data. (Gray spheres represent the Mn^{3+} cations and the black arrows show the approximate directions of the magnetic moments.)

deduced from it, are totally consistent with the observed NPD data. The 2 K refinement provides somewhat stronger evidence for partial oxidation than the 300 K data, and the oxygen site occupancies imply an overall stoichiometry of $Sr_3Mn_2O_{6.19(1)}$.

It is interesting to consider the origin of the partial vacancy order in the Mn layers around $z = \frac{1}{2}$, given that the $n = 1$ RP analog, $Sr_2MnO_{3.5}$, has a regular repeat of the translation vector between adjacent layers of MnO_5 square pyramids, and the resulting symmetry is therefore monoclinic. Both the nuclear and magnetic structure determinations described here strongly support long-range ordering of the O vacancies within and between the bilayers of MnO_5 square pyramids that are located in the basal plane of the unit cell. There is also long range order between the layers at $z = 0$ and 1, separated by ~ 20 Å, such that the vacancies are located directly above each other in these layers. It is possible that a domain structure exists, in which different domains have different translations for the layers at $z = \frac{1}{2}$. However, since the bilayers at $z = 0$ and those at $z = \frac{1}{2}$

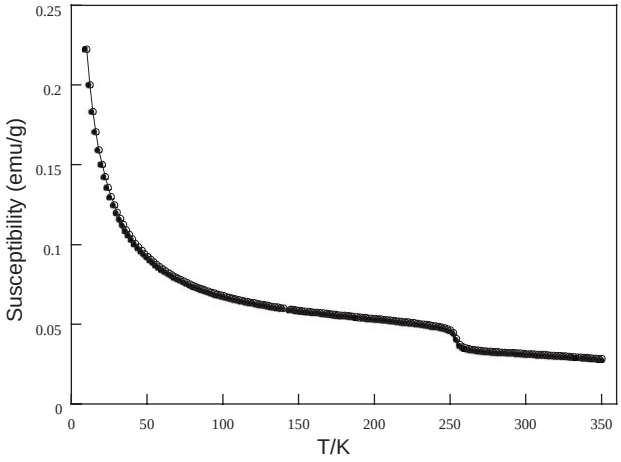

Fig. 10. Mass susceptibility vs. temperature plot of $Sr_3Mn_2O_6$ in an applied field of 1000 G. (No difference was observed between ZFC and FC data sets.)

are chemically equivalent, it is not clear to see the rationale for their differentiation structurally. Preferential occupancy of alternate bilayers by the additional oxygen that appears to be present would provide a plausible solution, but the NPD refinements provide no evidence for significant differences between the oxygen contents of the manganese oxide layers. It appears as though there exists reasonably large ordering enthalpies within the bilayers and between alternate bilayers; partial disorder within the sandwiching layers may occur in order to relieve possible strain which may result in a structure where all layers corresponding to $z = \frac{1}{2}$ are associated with a single translation, e.g. by $\pm\frac{1}{4}[\bar{1}00]$.

Magnetic susceptibility studies (χ) were carried out in an applied field of 1000 G. This revealed a transition at ca. 250 K with a small ferromagnetic contribution (Fig. 10) which is typical of materials having canted antiferromagnetic order. The data shown are the FC measurements only, since no difference was detectable between FC and ZFC data. However, due to the extremely complex magnetic structure, the nature of this small ferromagnetic component cannot be established by the NPD data.

4. Conclusions

The double-layered RP phase $Sr_3Mn_2O_{6+x}$ crystallizes with the oxygen vacancies forming an ordered array in the "MnO_2" layers of the perovskite blocks. The vacancies order to give a similar layer structure to $Sr_2MnO_{3.5}$ consisting of corner connected Jahn–Teller distorted MnO_5 square-based pyramids. The primitive tetragonal structure shows complete oxygen vacancy ordering in the perovskite block layers at $z = 0$ and 1, whereas only partial order is observed in the middle

layer at $z = \frac{1}{2}$. $Sr_3Mn_2O_{6+x}$ orders antiferromagnetically below ca. 250 K and the magnetic structure contains FM clusters aligned antiferromagnetically to each other within the perovskite block layers. The magnetic susceptibility data suggest a canted antiferromagnetic arrangement, but the canting is too small to be determined from the NPD data.

Acknowledgments

We thank EPSRC and IUAP 4 for financial support, and EPSRC for a studentship (LJG) and the provision of NPD facilities. We also thank Alan Hewat and Peter Cook for assistance in obtaining NPD data.

References

[1] Y. Moritomo, A. Asamitsu, H. Kuwahara, Y. Tokura, Nature 380 (1996) 141.
[2] P.D. Battle, M.A. Green, N.S. Laskey, J.E. Millburn, M.J. Rosseinsky, S. Sullivan, J.P. Vente, Chem. Comm. (1996) 767.
[3] N. Mizutani, A. Kitazawa, O. Nobuyuki, M. Kato, J. Chem. Soc. (Jpn.) Ind. Ed. 73 (1970) 1097.
[4] J.F. Mitchell, J.E. Millburn, M. Medarde, S. Short, J.D. Jorgensen, J. Solid State Chem. 141 (1998) 599.
[5] J.F. Mitchell, J.E. Millburn, M. Medarde, D.M. Argyriou, J.D. Jorgensen, J. Appl. Phys. 85 (1999) 4352.
[6] I. Guedes, J.F. Mitchell, D. Argyriou, M. Grimsditch, Phys. Rev. B 62 (2000) 13809.
[7] I. Guedes, J.F. Mitchell, D. Argyriou, M. Grimsditch, J. Magn. Magn. Mater. 226–230 (2001) 1998.
[8] L.J. Gillie, A.J. Wright, J. Hadermann, G. Van Tendeloo, C. Greaves, J. Solid State Chem. 167 (2002) 145.
[9] A.C. Larson, R.B. Von Dreele, General Structure Analysis System, Los Alamos National Laboratory, Los Alamos, NM, 1994.
[10] V. Caignaert, N. Nguyen, A. Ducouret, M. Hervireu, B. Raveau, Mater. Res. Bull. 20 (1985) 479.
[11] V. Caignaert, J. Magn. Magn. Mater. 166 (1997) 117.
[12] J.B. Goodenough, Magnetism and the Chemical Bond, VCH-Wiley, New York, 1963.
[13] J. Kanamori, J. Phys. Chem. Solids 10 (1959) 87.